北見工業大学研究報告　　Memoirs of the Kitami Institute of Technology
第20巻　第1号（昭和63年）　　Vol. 20 No. 1 (1988)

Dynamic Kinetics of N_2O–CO Reaction on Magnesium Oxide with Multifunctional Active Sites*

by Hidemi OHASHI**, Tohru KANNO***, Toshihide HIDA****, Takanobu ONOSE***** and Masayoshi KOBAYASHI***

(Received April 26, 1988)

Abstract

The heterogeneously catalysed N_2O–CO reaction was carried out on magnesium oxide with multifunctional active sites at 290–320°C by using an ordinary tubular flow reactor under atmospheric pressure, and the transient state of reaction was analysed by the transient response method. The steady state analysis of the reaction revealed the first order with respect to the concentration of carbon monoxide and zeroth order with respect to the concentration of nitrous oxide. Three different active sites were considered on the catalyst surface named S_1, S_2 and S_3. CO and CO_2 were competitively adsorbed on S_1, and coadsorbed CO+CO_2 interacted strongly with each other. N_2O was decomposed on S_2 and reacted with gaseous CO to produce CO_2. 98% of the surface sites were occupied by S_3 which is presumed to be a subactive site for the surface diffusion of adsorbed species.

The computer simulation technique using a personal computer was effectively applied to study the reaction mechanism. A possible mathematical model to analyse the proposed mechanism was presented, and a large number of transient response curves based on many different reaction sequences were simulated and referred to the experimental response curves. The model of the response curves were compared, and a possible reaction mechanism was proposed.

1. Introduction

Magensium oxide has been well known as a less active catalyst for the decomposition of nitrous oxide and carbon monoxide oxidation[1~9]. Actually it has, however, been confirmed to be active for CO oxidation at temperatures higher than 150°C as we previously reported.[10,11] In addition, the adsorption and desorption of CO and CO_2 show extremely interesting behavior because of the multifunctional nature of the surface such as basidity, acidity and a variety of coordinate unsaturation.[12~14] The multifunctional nature of magnesium oxide induces variety in the activity of the adsorbed species some of which are true intermediate for CO oxidation, and others which have a role as subspecies relating to the reaction route indirectly. The subspecies might control the surface diffusion

* The paper was presented at the Hokkaido regional meeting of the Chemical Society of Japan in 1985 and the national meeting of the Chemical Society of Japan in 1988.

** Chemical Environmental Engineering.
*** Department of Industrial Chemistry.
**** Japan Bureau of International Trade & Industry.
***** Hokkaido Sugar Co..

of the actual reaction intermediates during the reaction. Therefore, they are also important for the main route of the actual reaction.

The decomposition of nitrous oxide may basically be considered as a two step reaction[1~5,15] : (1) the decomposition of N_2O and (2) the desorption of oxygen formed. When CO is contained in the reaction gas mixture, it removes the oxygen species formed on the sites of N_2O decomposition, producing CO_2. If the CO_2 formed is desorbed very slowly, then the decomposition activity of N_2O will decrease quickly. Appreciable amounts of CO and CO_2 are adsorbed on MgO suggesting the presence of a large space for their adsorption as a reserver for the two gases. If the oxygen species formed by N_2O decomposition reacts with gaseous CO to produce CO_2 and the formed CO_2 migrates to a neighboring site which is for CO_2 or CO adsorption only, then the active sites for N_2O decomposition are always renewed. In this case, the catalytic activity can be kept stable.

In the present study, our interest focused on both (1) the identification of a variety of active sites on MgO and (2) the kinetic structure of the N_2O–CO reaction including the role of the active sites in the reaction sequences. The characterization of the active sites and the reaction mechanism were also studied by applying the transient response method[16,17], and the kinetic structure of the reaction was analysed by a computer simulation technique using a personal computer.

2. Experimental Procedure

The magnesium oxide used as a catalyst was commercially prepared by Wako Pure Chemical Co. The fine white powder of the sample was pressed at 2 ton/14.5 cm^2 for 5 min, and the disk formed was ground in an agate mortar so as to become 20~42 mesh. The sample contained such impurities as 0.005% Ba, 0.02% Zn, 0.005% As and 0.005% Fe. The BET surface area of the sample was measured to be 28 m^2/g by the adsorption of N_2 at −196°C.

The purities of gases used in this study were nitrous oxide (99.9% N_2O), oxygen (99.0% O_2), carbon monoxide (99.8% CO), carbon dioxide (99.5% CO_2) and helium (99.99% He). He was always passed through a Molecular Sieve 5A column which was cooled at −196°C by liquid nitrogen to remove oxygen as an impurity.

A gas chromatograph (TCD) was used to analyse the reaction gas composition. A Molecular Sieve 13 X column (2 m) was employed to analyse O_2, N_2 and CO, and a Porapak *Q* column (2 m) was used to analyse CO_2 and N_2O at 70°C.

5~61.8 g of catalyst were packed into a Pyrex glass tube reactor depending on the reaction conditions. The reactor was immersed into a fluidized sand bath the temperature of which was controlled within ±0.5°C. As a pretreatment of the catalyst, the sample was always treated in an He stream at 350°C for 20 hr prior to use in the experiment, refreshing the catalyst surface. The total gas flow rates were 80~160 ml (±2 ml) NTP/min depending on the reaction conditions which were always chosen so as to result in a total conversion of

less than 10%, because a differential reactor should be satisfied through the experiments.

For the computer simulation, two personal computers (NEC 8001 mkII) were used and the Runge-Kutta procedure was applied to solve the nonlinear differential equations.

3. Experimental Results and Discussion

3-1. Competitive Adsorption of CO, CO_2 and O_2

Fig. 2 illustrates the adsorption behavior of CO in two different conditions.

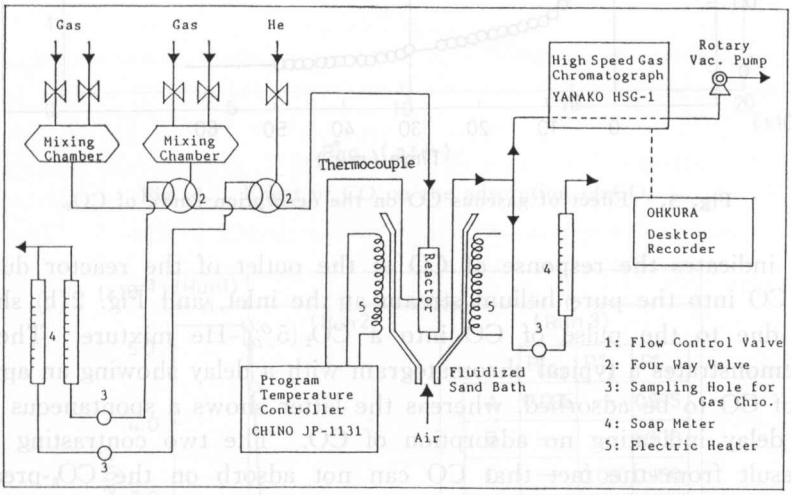

Fig. 1. Experimental apparatus.

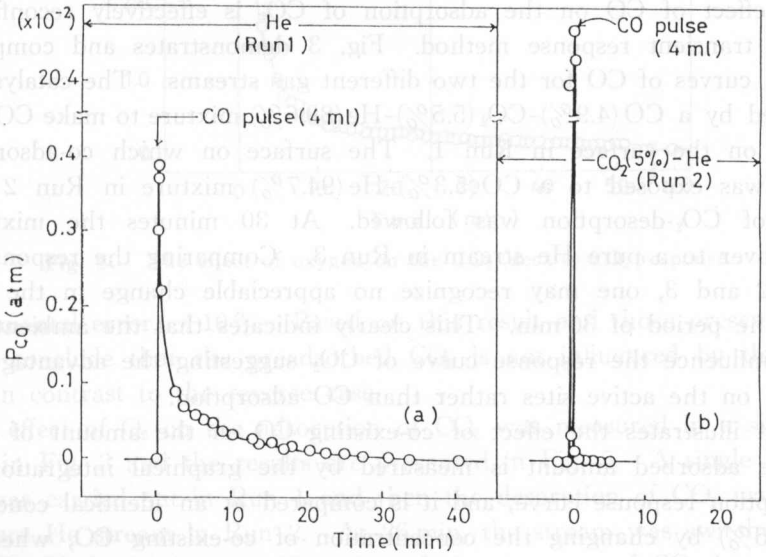

Fig. 2. Chromatographic responses of CO and CO_2 due to the pulse technique.

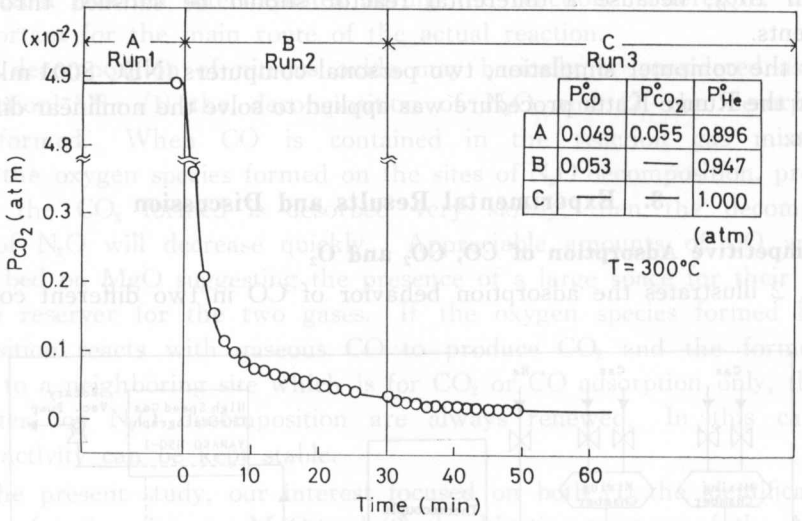

Fig. 3. Effect of gaseous CO on the desorption curve of CO_2.

Fig. 2 (a) indicates the response of CO at the outlet of the reactor due to the pulse of CO into the pure helium stream at the inlet, and Fig. 2 (b) shows the response due to the pulse of CO into a CO_2 (5%)-He mixture. The former clearly demonstrates a typical chromatogram with a delay showing an appreciable amount of CO to be adsorbed, whereas the latter shows a spontaneous response with no delay indicating no adsorption of CO. The two contrasting response curves result from the fact that CO can not adsorb on the CO_2-preadsorbed surface. The adsorption of CO_2 might be stronger than that of CO and the rate of CO_2 adsorption be faster than that of CO.

The effect of CO on the adsorption of CO_2 is effectively reconfirmed by using the transient response method. Fig. 3 demonstrates and compares the desorption curves of CO for the two different gas streams. The catalyst surface was treated by a CO (4.9%)-CO_2 (5.5%)-He (89.6%) mixture to make CO and CO_2 co-adsorb on the surface in Run 1. The surface on which co-adsorbing CO and CO_2 was exposed to a CO (5.3%)-He (94.7%) mixture in Run 2 and the response of CO_2-desorption was followed. At 30 minutes the mixture was switched over to a pure He stream in Run 3. Comparing the response curves of Runs 2 and 3, one may recognize no appreciable change in the response curve at the period of 30 min. This clearly indicates that the ambient CO gas does not influence the response curve of CO_2 suggesting the advantage of CO_2 adsorption on the active sites rather than CO adsorption.

Fig. 4 illustrates the effect of co-existing CO on the amount of adsorbed CO_2. The adsorbed amount is measured by the graphical integration of the CO_2-desorption response curve, and it is compared at an identical concentration of CO_2 (0.5%) by changing the concentration of co-existing CO, where He is used as a balance gas. The amount of CO_2 measured falls within the fluctuation

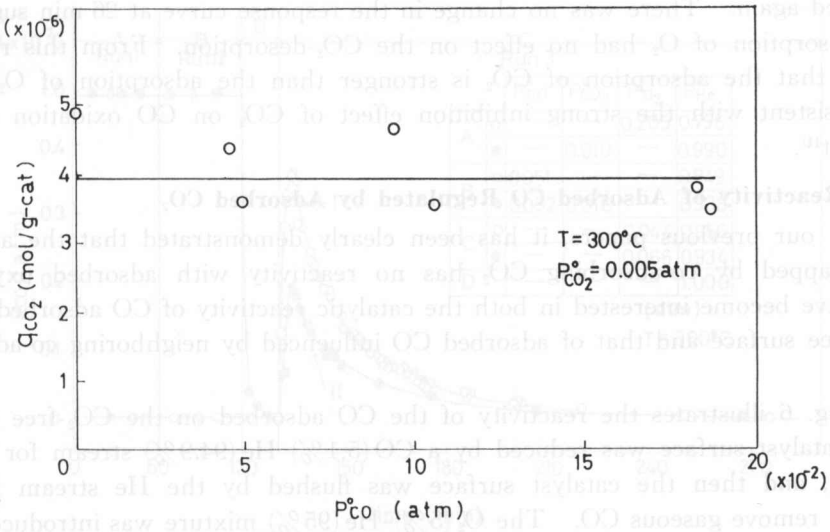

Fig. 4. Effect of CO on the adsorption of CO_2.

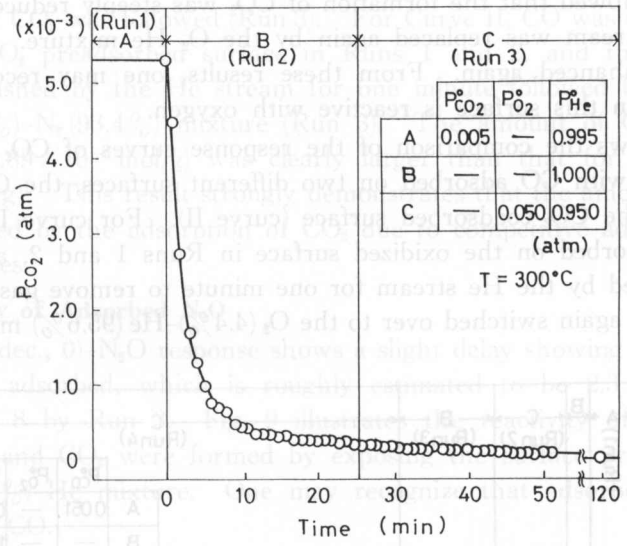

Fig. 5. The effect of oxygen on the CO_2 (dec., 0)–CO_2 response.

of experimental error, $\pm 10\%$. Based on this result and those presented above, one may conclude that the preadsorbed CO_2 is not influenced by the ambient CO gas in contrast to the reverse case.

The effect of O_2 on the adsorption of CO_2 was measured in a similar way to those in Fig. 3 and the results are presented in Fig. 5. A single adsorption of CO_2 was carried out in Run 1 and then the desorption of CO_2 was followed in the pure He stream in Run 2. At 26 min, the stream was switched over to the O_2 (5%)–He (95%) mixture (Run 3), and the response of CO_2-desorption was

followed again. There was no change in the response curve at 26 min suggesting the adsorption of O_2 had no effect on the CO_2-desorption. From this result, it seems that the adsorption of CO_2 is stronger than the adsorption of O_2. This is consistent with the strong inhibition effect of CO_2 on CO oxidation on this catalyst[11].

3-2. Reactivity of Adsorbed CO Regulated by Adsorbed CO_2

In our previous papers, it has been clearly demonstrated that the adsorbed CO trapped by co-adsorbing CO_2 has no reactivity with adsorbed oxygen.[9,11] We have become interested in both the catalytic reactivity of CO adsorbed on the CO_2-free surface and that of adsorbed CO influenced by neighboring co-adsorbing CO_2.

Fig. 6 illustrates the reactivity of the CO adsorbed on the CO_2-free surface. The catalyst surface was reduced by a CO (5.1%)-He (94.9%) stream for 2 hr in Run 1, and then the catalyst surface was flushed by the He stream for one min to remove gaseous CO. The O_2 (5%)-He (95%) mixture was introduced stepwisely in Run 2. An appreciable amount of CO_2 was formed. At eleven minutes, the mixture was switched over to the pure He stream in Run 3. The response curve clearly showed that the formation of CO_2 was steeply reduced. At 24 min, the pure He stream was replaced again by the O_2-He mixture. The formation of CO_2 was enhanced again. From these results, one may recognize that the CO adsorbed on this surface is reactive with oxygen.

Fig. 7 shows the comparison of the response curves of CO_2 formed by the reaction of O_2 with CO adsorbed on two different surfaces, the CO_2-free surface (curve I) and the CO_2-coadsorbed surface (curve II). For curve I, the single gas of CO was adsorbed on the oxidized surface in Runs 1 and 2, and the surface was then flushed by the He stream for one minute to remove gaseous CO. The He stream was again switched over to the O_2 (4.4%)-He (95.6%) mixture and then

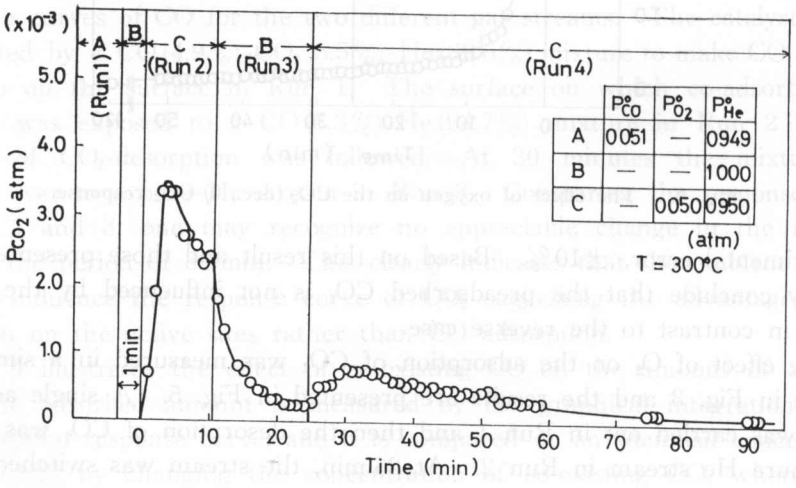

Fig. 6. Reactivity of adsorbed CO.

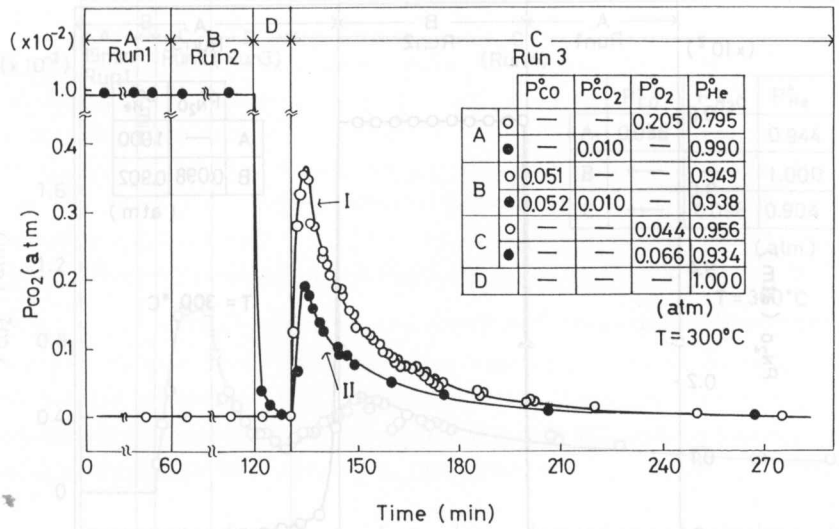

Fig. 7. Comparison of the reactivity of CO adsorbed on CO_2-free surface and CO_2-coexisting surface.

the response of CO_2 was followed (Run 3). For Curve II, CO was coadsorbed with CO_2 on the CO_2 preadsorbed surface in Runs 1 and 2, and then the catalyst surface was flushed by the He stream for one minute followed by the exposure to the O_2 (6.6%)–N_2 (93.4%) mixture (Run 3). The amount of CO_2 formed for Curve I ($q_I = 8.89 \times 10^{-6}$ mol/g) was clearly larger than that for Curve II ($q_{II} = 4.70 \times 10^{-6}$ mol/g). This result strongly demonstrates that the amount of adsorbed CO was reduced by the adsorption of CO_2 due to competitive adsorption on the same active sites.

3-3. Reactivity of Adsorbed N_2O

The N_2O (dec., 0)–N_2O response shows a slight delay showing a small amount of N_2O to be adsorbed, which is roughly estimated to be 2.3×10^{-8} mol/g, as shown in Fig. 8 by Run 3. Fig. 9 illustrates the reactivity of adsorbed N_2O with CO. N_2 and CO_2 were formed by exposing the surface preadsorbing N_2O to the CO (5.3%)–He mixture. One may recognize that adsorbed N_2O has no reactivity with CO.

Let us consider the reactivity of gaseous N_2O with adsorbed CO. Fig. 10 shows the transient response of CO_2 formed by the reaction of adsorbed CO with gaseous N_2O. The catalyst surface was reduced by the CO (5.6%)–He (94.4%) mixture for 15 min and the reactor was then flushed by the pure He for one minute followed by the introduction of the N_2O (9.6%)–He (90.4%) mixture (see Run 2). Run 2 clearly shows that the production of CO_2, and the rate of CO_2 formation is decreased by the successive He flushing of the reactor as shown in Run 3. When the He stream is switched back to the N_2O–He mixture, CO_2 is formed again slowly in Run 4. The series of these transient experiments clearly shows adsorbed CO to be reactive with gaseous N_2O.

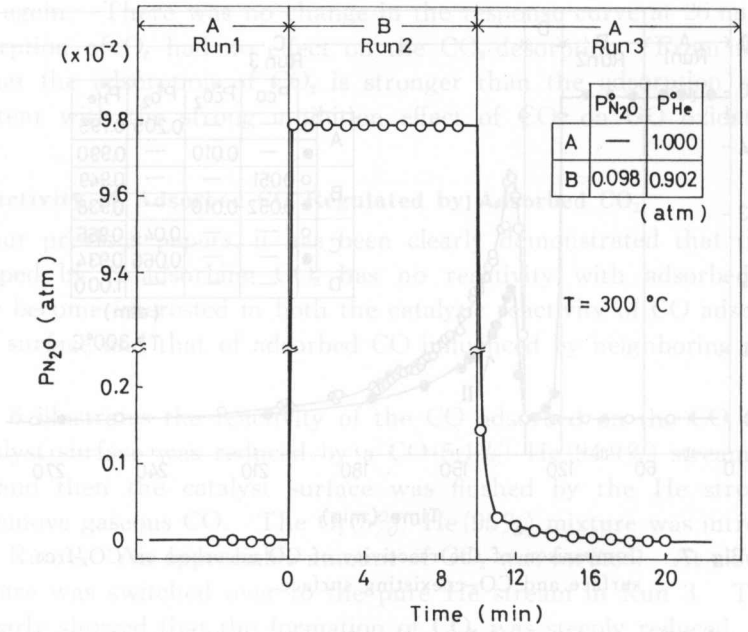

Fig. 8. N_2O–N_2O response.

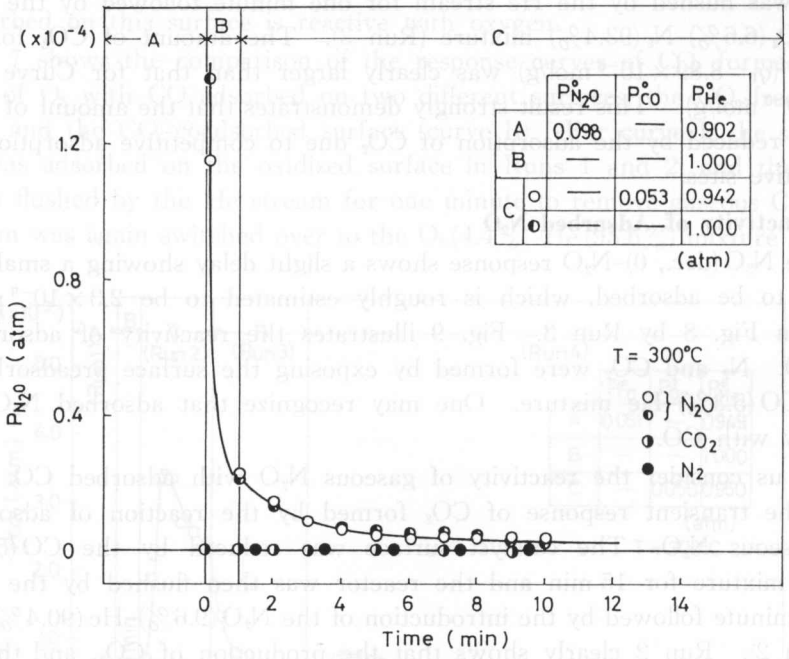

Fig. 9. Reactivity of adsorbed N_2O with CO.

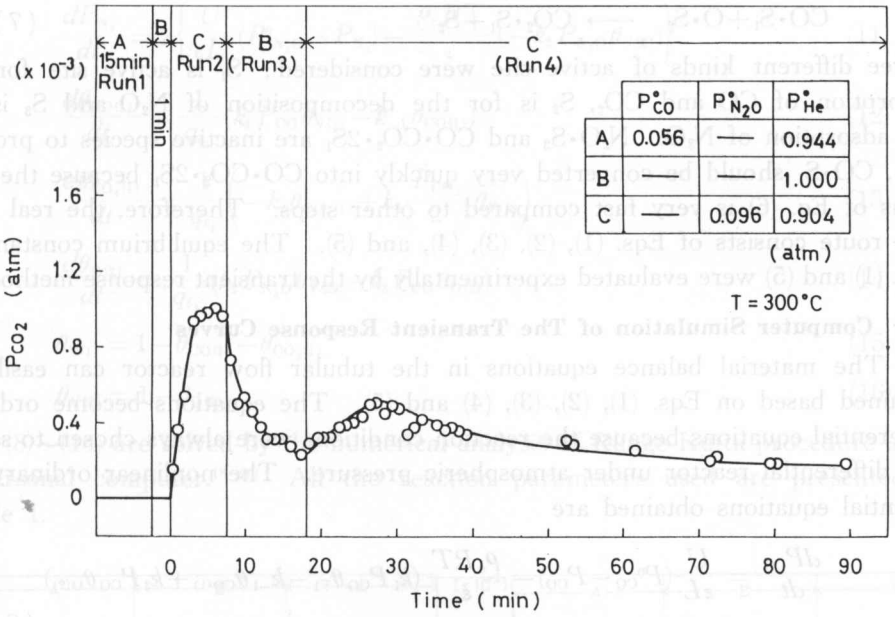

Fig. 10. Reactivity of the adsorbed CO with N_2O.

In our previous papers, adsorbed CO has no reactivity with O_2 and N_2O when CO_2 coexists in the gas phase because of the trapping effect of CO_2 on CO. During the N_2O–CO reaction, since CO_2 formed by the reaction coexists in a gas phase even though less than $P_{CO_2}=0.01$ atm, the adsorbed CO should not be reactive with N_2O during the N_2O–CO reaction. Therefore, atomic oxygen formed by the decomposition of N_2O can react with gaseous CO excluding the possibility of the reaction of adsorbed CO with N_2O.

3-4. Reaction Mechanism

Based on the experimental results obtained so far, the following reaction mechanism may be proposed

$$CO\,(g)+S_1 \underset{k_{-1}}{\overset{k_1}{\rightleftharpoons}} CO\cdot S_1 \qquad (1)$$

$$N_2O\,(g)+S_2 \xrightarrow{k_2} O\cdot S_2+N_2\,(g) \qquad (2)$$

$$N_2O\,(g)+S_3 \rightleftharpoons N_2O\cdot S_3 \qquad (3)$$

$$CO\,(g)+O\cdot S_2 \xrightarrow{k_3} CO_2\,(g)+S_2 \qquad (4)$$

$$CO_2\,(g)+S_1 \underset{k_{-4}}{\overset{k_4}{\rightleftharpoons}} CO_2\cdot S_1 \qquad (5)$$

$$CO_2\cdot S_1+CO\cdot S_1 \rightleftharpoons CO\cdot CO_2\cdot 2S_1 \quad \text{(inactive)} \qquad (6)$$

$$CO \cdot S_1 + O \cdot S_2 \longrightarrow CO_2 \cdot S_1 + S_2 \qquad (7)$$

Three different kinds of active site were considered: S_1 is active site for the adsorption of CO and CO_2, S_2 is for the decomposition of N_2O and S_3 is for the adsorption of N_2O. $N_2O \cdot S_3$ and $CO \cdot CO_2 \cdot 2S_1$ are inactive species to produce CO_2, $CO \cdot S_1$ should be converted very quickly into $CO \cdot CO_2 \cdot 2S_1$ because the progress of Eq. (6) is very fast compared to other steps. Therefore, the real reaction route consists of Eqs. (1), (2), (3), (4), and (5). The equilibrium constants of Eqs. (1) and (5) were evaluated experimentally by the transient response method.[16,17]

3-5. Computer Simulation of The Transient Response Curves

The material balance equations in the tubular flow reactor can easily be obtained based on Eqs. (1), (2), (3), (4) and (5). The equations become ordinary differential equations because the reaction conditions were always chosen to satisfy the differential reactor under atmospheric pressure. The nonlinear ordinary differential equations obtained are

$$\frac{dP_{CO}}{dt} = \frac{U}{\varepsilon L}(P^0_{CO} - P_{CO}) - \frac{\rho_c RT}{\varepsilon}(k_1 P_{CO}\theta_{V1} - k_{-1}\theta_{CO(1)} + k_3 P_{CO}\theta_{O(2)}) \qquad (8)$$

$$\frac{dP_{N_2O}}{dt} = \frac{U}{\varepsilon L}(P^0_{N_2O} - P_{N_2O}) - \frac{\rho_c RT}{\varepsilon}(k_2 P_{N_2O}\theta_{V1}) \qquad (9)$$

$$\frac{dP_{CO_2}}{dt} = 2\left\{\frac{U}{\varepsilon L}(P^0_{CO_2} - P_{CO_2}) - \frac{\rho_c RT}{\varepsilon}(k_3 P_{CO}\theta_{O(2)} - k_4\theta_{CO_2(1)} + \frac{k_{-4}}{2}\theta_{CO_2(1)} + k_4\frac{P_{CO_2}}{2}\theta_{V(1)})\right\} \qquad (10)$$

Table 1. Summary of the reaction parameters used for the computer simulation.

Run	T °K	U cm/min	L cm	ε (—)	ρ_c g/cm³	q_{CO} mol/g	q_O mol/g	q_{CO_2} mol/g	k_1	k_2	k_3	k_4	K_1 atm⁻¹	K_4 atm⁻¹
a	573	318.3	120	0.645	1.03	8.54×10^{-6}	1.37×10^{-6}	6.67×10^{-6}	1.0×10^{-3}	1.5×10^{-3}	2.72×10^{-5}	1.0×10^{-5}	202	254
b									1.0×10^{-2}			1.0×10^{-7}		
c									1.0×10^{-2}			1.0×10^{-6}		
d									2.63×10^{-4}			3.5×10^{-5}		
e									4.0×10^{-3}			5.0×10^{-7}		
f									5.0×10^{-4}			5.0×10^{-6}		
g	583								7.15×10^{-3}	2.79×10^{-3}	2.72×10^{-5}	7.14×10^{-6}	127	347
h	593								1.0×10^{-2}	5.0×10^{-3}	3.1×10^{-5}	1.0×10^{-5}	82.5	286
i	563								3.59×10^{-3}	8.3×10^{-4}	2.5×10^{-5}	3.51×10^{-6}	335	363
j	573								5.0×10^{-3}	1.5×10^{-3}	2.72×10^{-5}	5.0×10^{-6}	202	445

$$\frac{dP_{N_2}}{dt}=2\left\{\frac{U}{\varepsilon L}(P^0_{N_2O}-P_{N_2})-\frac{\rho_c RT}{\varepsilon}(-k_2 P_{N_2O}\theta_{V(2)})\right\} \tag{11}$$

$$\frac{d\theta_{CO(1)}}{dt}=\frac{1}{q_{t_1}}(k_1 P_{CO}\theta_{V(1)}-k_{-1}\theta_{CO(1)}) \tag{12}$$

$$\frac{d\theta_{CO_2(1)}}{dt}=\frac{1}{q_{t_2}}\left(-k_4\theta_{CO_2(1)}+k_4\frac{P_{CO_2}}{2}\theta_{V(1)}\right). \tag{13}$$

$$\frac{d\theta_{O(2)}}{dt}=\frac{1}{q_{t_3}}(k_2 P_{N_2O}\theta_{V(2)}-k_3 P_{CO}\theta_{O(3)}) \tag{14}$$

$$\theta_{V(1)}=1-\theta_{CO(1)}-\theta_{CO_2(1)} \tag{15}$$

$$\theta_{V(2)}=1-\theta_{O(2)} \tag{16}$$

Eqs. (8)~(14) are solved by the numerical analysis of Runge-Kutta procedure using a personal computer.[18~20] All the reaction parameters used are presented in Table 1.

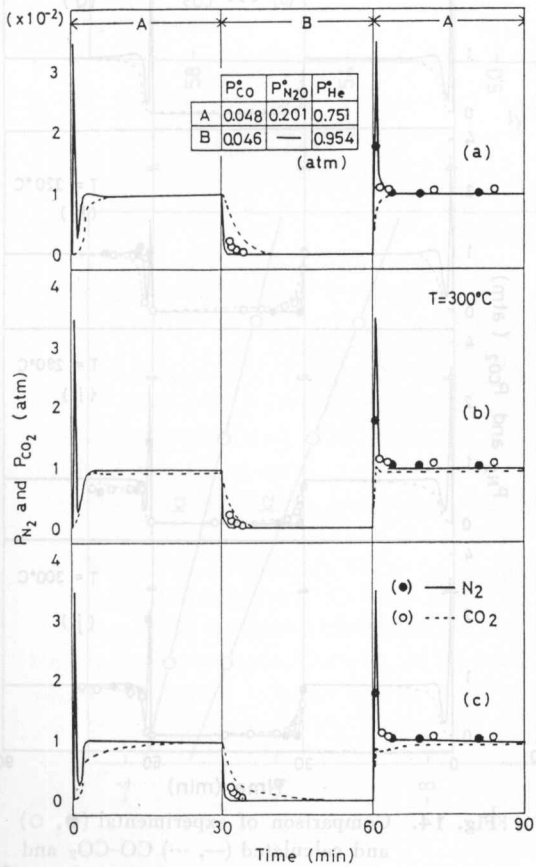

Fig. 11. Comparison of experimental (●, ○) and calculated (—, ···) CO–CO_2 and –N_2 responses.

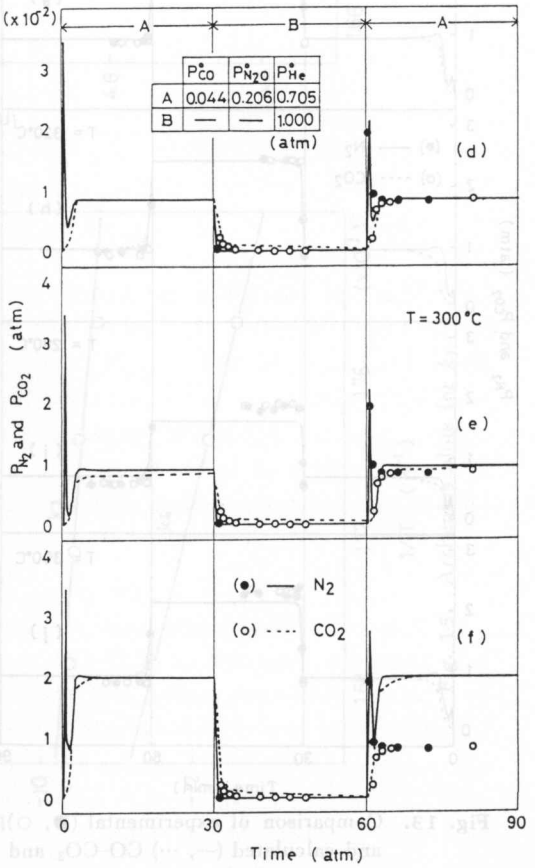

Fig. 12. Comparison of experimental (●, ○) and calculated (—, ···) CO–CO_2 and –N_2 responses.

Fig. 11 illustrates the sensitivity of the rate constants k_j affecting the mode of the transient response curves when the gas composition is changed stepwisely between the CO (4.8%)-N_2O (20.1%)-He (75.1%) mixture and the pure He stream. k_4 is changed between 10^{-5} and 10^{-7} (see Fig. 11 (a), (b) and (c)) and no appreciable change is observed especially at the steady state levels of CO_2 and N_2, showing no good agreement with the experimental curves. k_1 and k_4 then are simultaneously changed to find fitting value and the results are presented in Fig. 12 (d), (e) and (f). None of the results are in satisfactory agreement with the experimental curves. Finally, one can conclude that there are no fitting values at $K_1=202$ and $K_4=254\ \text{atm}^{-1}$. To get more reasonable results, K_1 and K_4 should be changed.

A large number of the kinetic parameter sets were tested to find the values best fitting the experimental curves and the results are presented in Figs. 13 and

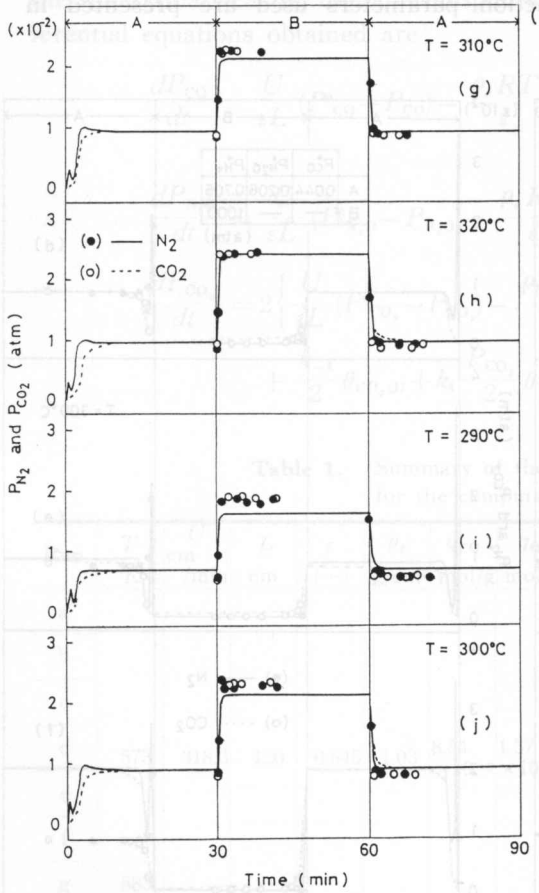

Fig. 13. Comparison of experimental (●, ○) and calculated (—, ···) CO–CO_2 and –N_2 responses.
A : CO (4.4%)-N_2O (20.6%)-He (75.0%)
B : CO (10.7%)-N_2O (19.8%)-He (69.5%)

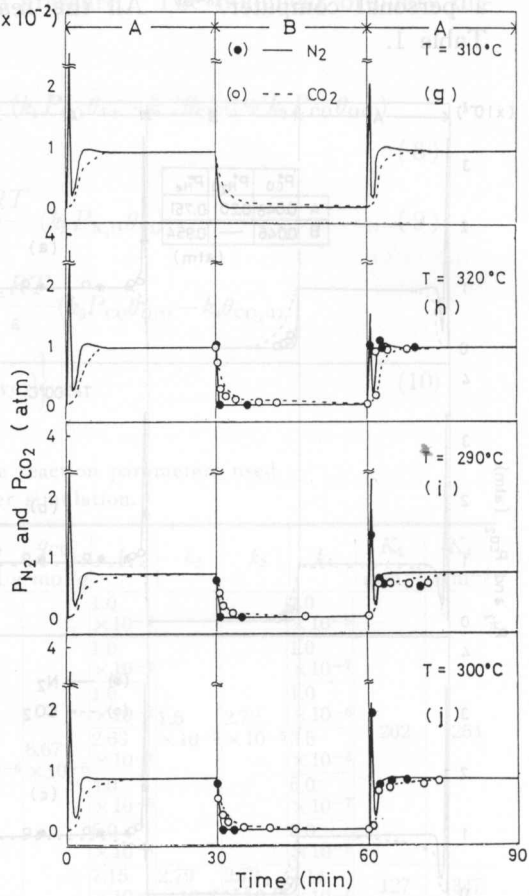

Fig. 14. Comparison of experimental (●, ○) and calculated (—, ···) CO–CO_2 and –N_2 responses.
A : CO (4.4%)-N_2O (20.6%)-He (75.0%)
B : He (100.0%)

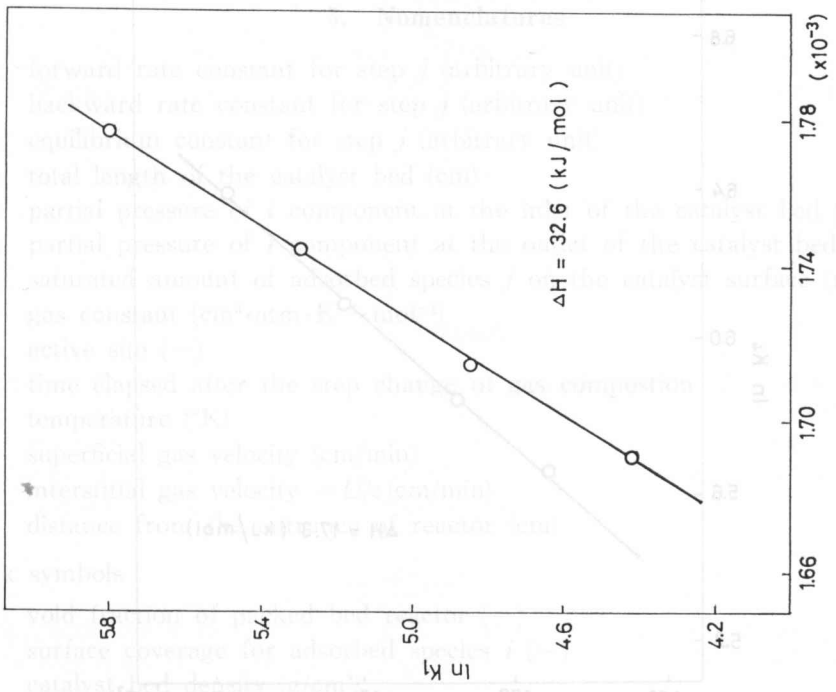

Fig. 16. Plots of $\ln K_1$ vs. $1/T$.

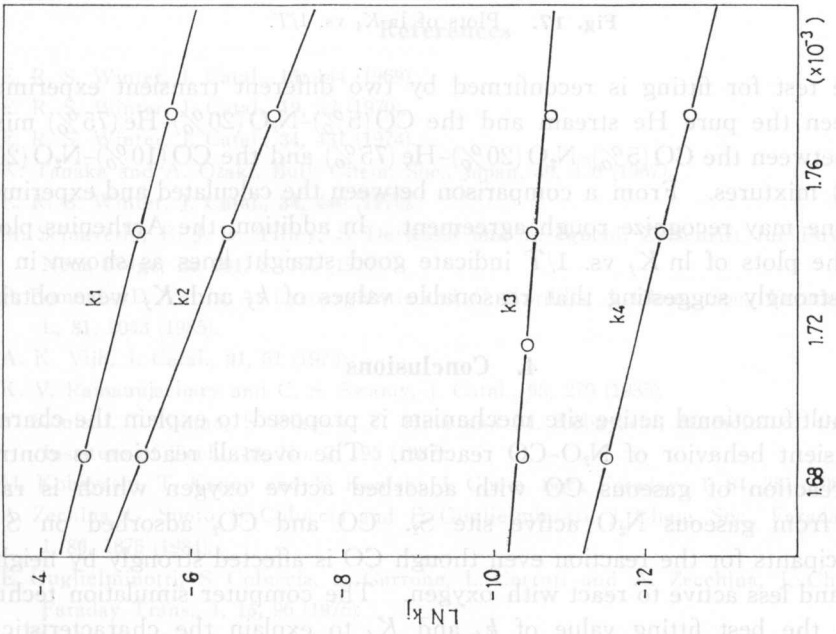

Fig. 15. Arrhenius plots for k_j.

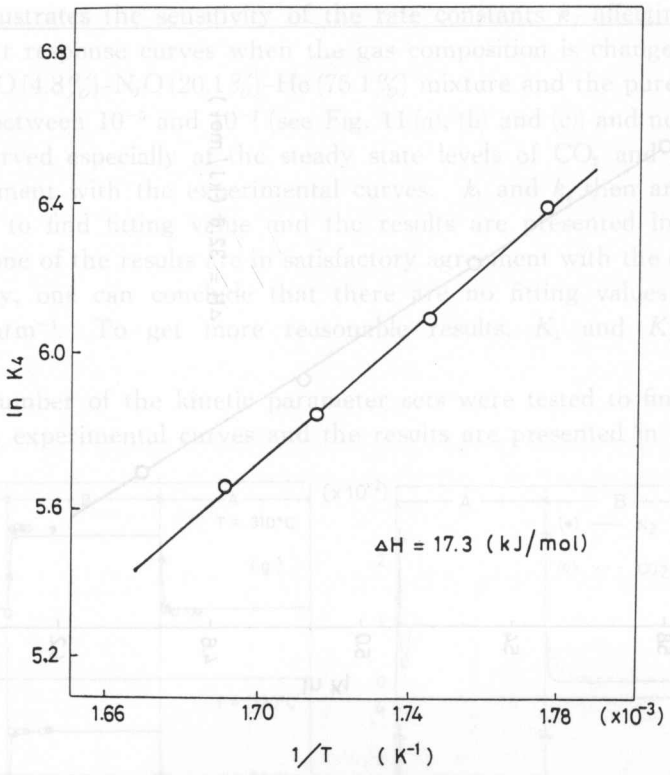

Fig. 17. Plots of $\ln K_4$ vs. $1/T$.

14. The test for fitting is reconfirmed by two different transient experiments: (1) between the pure He stream and the CO (5%)-N_2O (20%)-He (75%) mixture and (2) between the CO (5%)-N_2O (20%)-He (75%) and the CO (10%)-N_2O (20%)-He (70%) mixtures. From a comparison between the calculated and experimental curves, one may recognize rough agreement. In addition, the Arrhenius plots of k_j and the plots of $\ln K_j$ vs. $1/T$ indicate good straight lines as shown in Figs. 15~17, strongly suggesting that reasonable values of k_j and K_j were obtained.

4. Conclusions

A multifunctional active site mechanism is proposed to explain the characteristic transient behavior of N_2O-CO reaction. The over-all reaction is controlled by the reaction of gaseous CO with adsorbed active oxygen which is rapidly supplied from gaseous N_2O active site S_2. CO and CO_2 adsorbed on S_1 are not participants for the reaction even though CO is affected strongly by neighboring CO_2 and less active to react with oxygen. The computer simulation technique evaluates the best fitting value of k_j and K_j to explain the characteristic transient response curves obtained.

5. Nomenclatures

k_j : forward rate constant for step j (arbitrary unit)
k_{-j} : backward rate constant for step j (arbitrary unit)
K_j : equilibrium constant for step j (arbitrary unit)
L : total length of the catalyst bed (cm)
P_i^0 : partial pressure of i component at the inlet of the catalyst bed (atm)
P_i : partial pressure of i component at the outlet of the catalyst bed (atm)
q_j : saturated amount of adsorbed species j on the catalyst surface (mol/g)
R : gas constant ($cm^3 \cdot atm \cdot K^{-1} \cdot mol^{-1}$)
S : active site (−)
t : time elapsed after the step change of gas compostion
T : temperature (°K)
U : superficial gas velocity (cm/min)
U_i : interstitial gas velocity $= U/\varepsilon$ (cm/min)
Z : distance from the entrance of reactor (cm)

Greek symbols

ε : void fraction of packed bed reactor (−)
θ_i : surface coverage for adsorbed species i (−)
ρ_c : catalyst bed density (g/cm^3)
ρ_M : molar density (mol/cm^3)

References

1) E. R. S. Winter, J. Catal., **15**, 144 (1969).
2) E. R. S. Winter, J. Catal., **19**, 32 (1970).
3) E. R. S. Winter, J. Catal., **34**, 431 (1974).
4) K. Tanaka and A. Ozaki, Bull. Chem. Soc., Japan, **40**, 420 (1967).
5) E. R. S. Winter, J. Catal., **34**, 440 (1974).
6) M. Schiavellp, R. J. D. Tilley, S. De Rossi and E. Iguchi, Zefschrift fur Phys. Chem. Neue Folge, Ba **104**, S. 165 (1977).
7) P. Pomonis, D. Vattis, A. Lycovrghiotis and C. Kordilis, J. Chem. Soc., Faraday Trans., L, **81**, 2043 (1985).
8) A. K. Vijh, J. Catal., **31**, 51 (1973).
9) K. V. Ramanujachary and C. S. Swamy, J. Catal., **93**, 279 (1985).
10) Y. Konishi, T. Kanno, S. Oikawa, T. Hida and M. Kobayashi, Memoirs of the Kitami Institute of Tech., **18**, No. 2, 195 (1987).
11) M. Kobayashi, T. Kanno and Y. Konishi, J. Chem. Soc., Faraday., 1, **84**, 281 (1988).
12) A. Zechina, G. Spoto, S. Coluccia and E. Guglielminotti, J. Chem. Soc., Faraday Trans., 1, **80**, 1875 (1984).
13) E. Guglielminotti, S. Coluccia, E. Garrone, L. Cerruti and A. Zecchina, J. Chem. Soc., Faraday Trans., 1, **15**, 96 (1975).
14) A. Zecchina and F. S. Stone, J. Chem. Soc., Faraday Trans., 1, **74**, 2280 (1978).
15) M. Kobayashi and H. Kobayashi, J. Chem. Eng. Japan, **6**, 438 (1983).
16) H. Kobayashi and M. Kobayashi, Catal. Rev. Eng. Sci., **10**, 139 (1975).
17) C. O. Bennett, Catal. Rev. Eng. Sci., **12**, 105 (1976).

18) M. Kobayashi, Chem. Eng. Sci., **39**, 393 (1982).
19) T. Kanno, T. Kimura, T. Onose, M. Hayashi and M. Kobayashi, Memoirs of the Kitami Institute of Tech., **19**, No. 1, 71 (1987).
20) M. Kobayashi, Y. Maeda and N. Takahashi, J. Chem. Tech. Biotechnology, **33 A**, 219 (1983).